INORGANIC CHEMISTRY
FRONTIERS

RESEARCH ARTICLE

View Article Online
View Journal | View Issue

Cite this: *Inorg. Chem. Front.*, 2020, **7**, 2370

Anthracene–styrene-substituted *m*-carborane derivatives: insights into the electronic and structural effects of substituents on photoluminescence†

Mahdi Chaari, [a] Zsolt Kelemen, [a] Duane Choquesillo-Lazarte, [b] Francesc Teixidor, [a] Clara Viñas [a] and Rosario Núñez *[a]

Two anthracenyl–styrenyl-*m*-carborane triads (one non-iodinated on B, **3**, and one iodinated, **4**) were synthesized and characterized to be further linked to octavinylsilsesquioxane (OVS) *via* cross-metathesis, giving rise to the corresponding hybrid materials **5** and **6**. The crystal structure of the non-iodinated heterosubstituted-*m*-carborane **3** was analyzed by X-ray diffraction. Transmission electron microscopy images of pristine OVS and hybrids **5–6** show important differences in the morphology of the particles; whereas OVS forms cubic-like particles, **5–6** have a spherical shape with a broad particle-size distribution. All compounds showed similar vibronic emission spectra in solution, with maxima around 415 nm, assigned to the locally excited state (LE) emission of the anthracene moiety. The similarity with the spectra of the free anthracene (λ_{em} = 420 nm) suggested that only small electronic interactions between the anthracene units have taken place, and there is no influence of the iodo or styrene groups on the absorption properties. This is in agreement with the DFT calculations, where calculated oscillator strength corresponding to the transitions from iodo orbitals to the LUMO are weak and could not be observed experimentally. Noticeable, triads **3–4** exhibited exceptional fluorescence quantum yield values of around 100% in solution, that are comparable to those determined for their precursors **1–2**, demonstrating that the influence of the styrene group is negligible. Linking these *m*-carborane derivatives to the OVS led to a significant decrease of quantum yields to 34–45% for **5–6** in solution. Moreover, the PL behavior in the aggregate state was investigated and the spectra of all compounds were very similar, showing emission red-shift with maxima around 455–459 nm. Remarkably, quite high fluorescence quantum yields were determined for **3–4** (ϕ_F = 26–31%) and **5–6** (ϕ_F = 27–36%) in the aggregated state. These data confirm that the *m*-carborane platform enhances the quantum efficiency of the anthracene in solution, without losing the emission properties in the aggregate state. If this affirmation is associated to other scattered examples on other fluorophores also linked to *m*-carborane existing in the literature, the former conclusion is reinforced. *m*-Carborane enhances the fluorescence quantum yield of the free fluorophore, but does not alter the energy of the participating states in the photoluminescence in solution.

Received 30th January 2020,
Accepted 8th May 2020

DOI: 10.1039/d0qi00127a

rsc.li/frontiers-inorganic

Introduction

Optoelectronic organic materials have been successfully applied in organic light-emitting diodes (OLEDs), thin-film-transistors, electrochromic devices, sensors, liquid crystal displays, among others, due to their low-cost, facile processability, variability in structural and property tuning, and the capability of producing large areas of a flexible thin film.[1]

The incorporation of polyhedral oligomeric silsesquioxanes (POSSs) into optoelectronic materials to achieve improved performances has attracted particular attention due to the unique and interesting hybrid structures of POSS. In particular, octasilsesquioxanes are nanosized building blocks for organic/in-

[a]*Institut de Ciència de Materials de Barcelona (ICMAB-CSIC), Campus U.A.B., 08193 Bellaterra, Barcelona, Spain. E-mail: rosario@icmab.es; Fax: +3493 580 5729; Tel: +34 93 580 1853*
[b]*Laboratorio de Estudios Cristalográficos, IACT-CSIC, Avda. de las Palmeras 4, 18100 – Armilla, Granada, Spain*

†Electronic supplementary information (ESI) available: ^{1}H, ^{11}B{^{1}H}, ^{13}C{^{1}H} NMR and IR-ATR spectra, computational details, crystallographic data and Hirshfeld surface analyses for all the compounds. CCDC 1972767. For ESI and crystallographic data in CIF or other electronic format see DOI: 10.1039/d0qi00127a

organic hybrid materials of general formulae $[RSiO_{1.5}]_8$ with a 3D scaffold that exhibit a huge versatility to be functionalized, high robustness and thermal stability.[2] They can be modified to tailor chemical, mechanical, electrical, optical or electronic properties.[3] These exceptional characteristics make them very useful for a wide variety of applications, including thermally and chemically resistant polymers and ceramics,[4] as flame retardants,[5] catalysis,[6] nanomedicine,[7] emitting layers in OLEDs,[8] among others.

Carboranes are icosahedral clusters of formula $C_2B_{10}H_{12}$,[9] with three-dimensional (3D) σ-delocalization,[10] and electron-acceptor ability through substitution at the $C_{cluster}$ (C_c).[11] The linking of different fluorophores to the carborane C_c through a $-CH_2-$ spacer results in carborane-containing dyes, which fluorescence emission depends on the cluster isomer (*o*- or *m*-) and the substituent at the second C_c atom.[12d,13] It was also noticed that those dyes with low or null emission in solution were able to exhibit moderate fluorescence efficiency in the solid-state.[12d,14] In 2011, N. Hosmane *et al.* reported carborane-appended 1,3,5-triphenylbenzene (TB) and 1,3,5-tris (biphenyl-4-yl)benzene (TBB) containing three *o*-, *m*- and *p*-carborane clusters, showing that *o*-carborane produced a quenching of the fluorescence, whereas the *m*-isomer caused an increase of the fluorescence quantum yields (ϕ_F), from pristine TB (10%) and TBB (27%) to 25 and 46%, respectively, after bonding to *m*-carborane.[15] Their interpretation was that the 3D structure prevents the π–π stacking interactions in the π-conjugated systems and enhances rigidity of the conjugated molecules. Later, H. Yan observed that anthracene derivatives functionalized with *o*-carborane exhibited a ϕ_F of 5%, whereas its homologous one with the *m*-isomer yielded a ϕ_F of 94%, even higher that the starting anthracene derivative (70%).[16] These two examples were isolated cases and no further research was explored. Later, we also observed that *m*-carborane linked to stilbene groups achieves higher fluorescence efficiency than their homologous with *o*-carborane derivatives, being the ϕ_F values of *m*-carboranyl-stylbene 8–19% *vs.* *o*-carboranes (3–16%).[12d] So these isolated cases were moving into a general rule, but it had to be demonstrated more consistently. More recently, our group focused on *m*-carborane based anthracenes to demonstrate that triads of di-anthracenyl-*m*-carboranes gave quantum yield efficiencies of 63–66%, being in all cases significantly higher than the pristine anthracene (26%).[17a] Remarkably, when *m*-carborane is linked to only one anthracene to give C-monosubstituted compounds, the result is still more relevant and ϕ_F values close to 100% were obtained.[17b] Furthermore, for all of them, moderate to good quantum efficiencies in the aggregate state were also determined, demonstrating that *m*-carborane is a tool of choice to boost the photoluminescence (PL) properties of those organic π-conjugated systems bounded to it, as anthracenes, both in solution and solid-state.

Previously, our group has reported photoluminescent hybrid materials based on octasilsesquioxane cubic structures (POSS) decorated with terminal *o*-carborane clusters throughout organic π-conjugated systems.[18] The final PL properties of these hybrids may be tailored by changing the substituents at the C_c atoms. In these hybrids the POSS cage acts as an organizing scaffold, causing restriction to the intramolecular movement of the arms and avoiding additional interactions between them that could cause the quenching of the fluorescence (ϕ_F = 0.02–0.44).[18] Other sets of carboranyl-containing octasilsesquioxane hybrids were prepared linking *o*- and *m*-carborane to the POSS core by means of vinylstilbene units, exhibiting moderate to high fluorescent quantum yields in solution (ϕ_F = 0.21–0.59); being the most efficient, the one which contains non-substituted *o*-carborane units.[19] However, a quenching of the fluorescence was observed in the solid-state attributed to intermolecular interactions.

Throughout our research, we consistently have observed that when fluorophores are linked to *m*-carborane, the quantum yields are dramatically enhanced, many of them approaching 100%, and usually much higher than the plain fluorophores. In the current work, the *m*-carborane has been heterosubstituted at both C_c atoms with two different substituents, one fluorophore (the anthracene) that provides the PL properties, and one styrene, which enables the linking of our system to another platform, *i.e.* OVS. To gain further insight into the substituent effects at the *m*-carborane cluster on the PL properties of the final fluorophores, herein we analyse the photophysical properties in solution and aggregate states of two heterosubstituted anthracenyl–styrenyl-*m*-carborane clusters and their respective POSS hybrids, demonstrating that even by attaching a second substituent to the C_c of the *m*-carborane, the fluorescence efficiency is kept very high.

Results and discussion

Synthesis and characterization of compounds 3–6

To prepare fluorescence emitting boron rich hybrids we have followed the next strategy: in a first step, the synthesis of heterosubstituted anthracenyl–styrenyl-*m*-carborane triads was performed, followed by their linking to octavinylsilsesquioxane *via* cross-metathesis.

The starting anthracenyl-*m*-carborane derivatives **1–2** were prepared from 1,7-*closo*-$C_2B_{10}H_{12}$ and 9-I-1,7-*closo*-$C_2B_{10}H_{11}$,[17b,20] respectively, following literature procedures. Then, a second functionalization at the adjoining C_c–*H* was done by nucleophilic substitution of **1–2** using 15% of the excess of 4-vinylbenzyl chloride at reflux overnight,[12a] giving rise to heterosubstituted compounds **3** and **4**, in 61 and 67% yield, respectively (Scheme 1). This reaction was monitored by $^{11}B\{^1H\}$ NMR following the appreciable changes in the boron resonance distributions. In the second step, compounds **3** and **4** were reacted with the OVS *via* cross-metathesis, following the procedure previously reported by us,[18] using CH_2Cl_2 and the first generation of Grubbs catalyst,[21] to give hybrids **5** and **6**, in a 52 and 50% yield, respectively. The reaction was monitored by ^1H NMR and the complete conversion was confirmed upon a change in the aromatic proton resonance distributions, the disappearance of

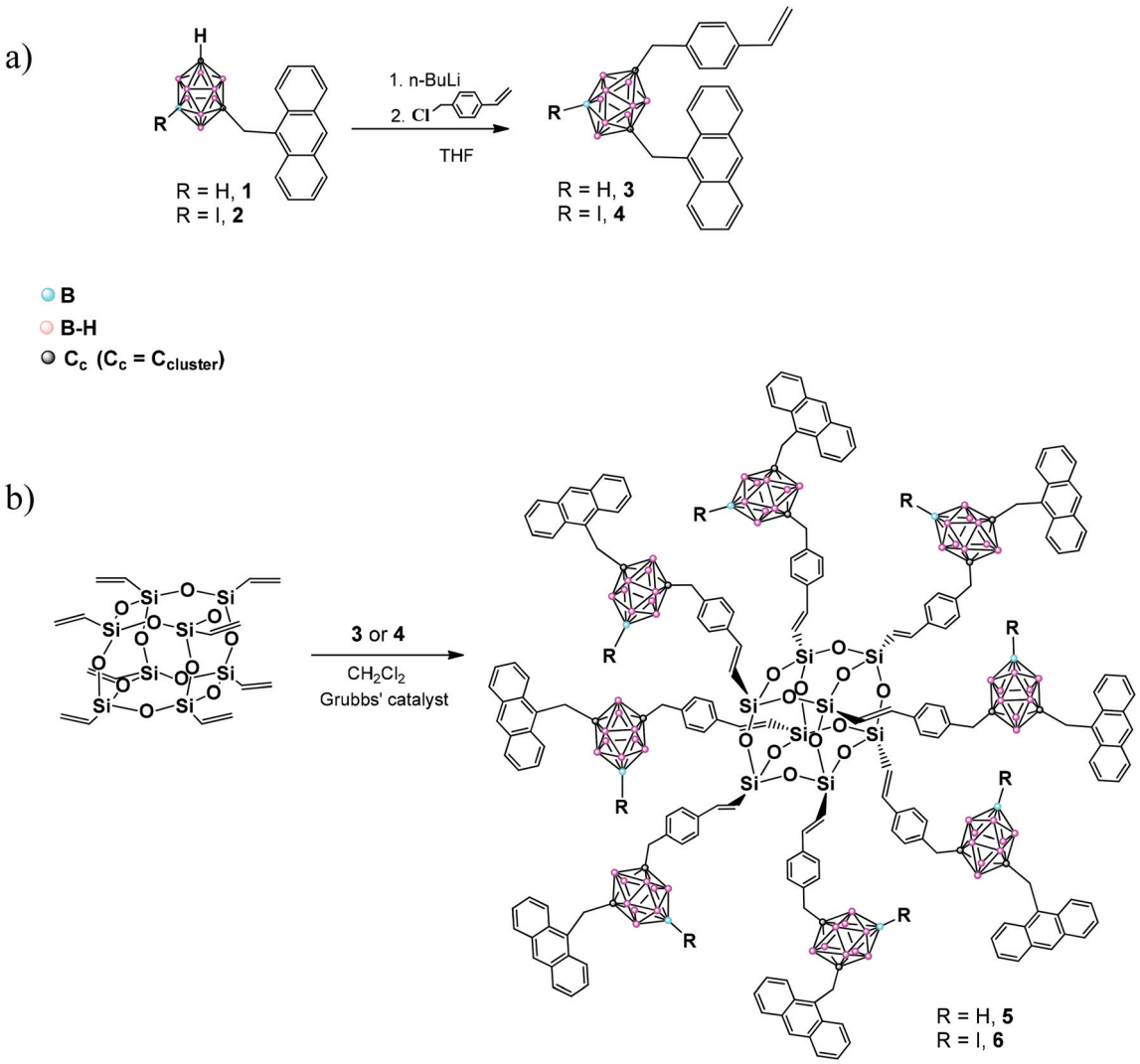

Scheme 1 Synthetic procedures for (a) compounds **3–4** and (b) hybrids **5–6**.

signals from the vinyl group, and the appearance of new resonances attributed to the two alkene protons.

The structures of **3–6** were established based on IR-ATR, ^{1}H, ^{13}C{^{1}H} and ^{11}B{^{1}H} NMR spectroscopy and elemental analysis; triad **3** was confirmed by X-ray diffraction analysis. The IR-ATR spectra of all compounds show typical ν(B–H) strong bands of *closo*-clusters between 2557 and 2596 cm^{-1}. The IR-ATR spectra of **5–6** show a band near 1600 cm^{-1} attributed to the ν(C=C) and the typical broad band around 1085 cm^{-1} due to the Si–O bond. ^{1}H NMR spectra of **3–4** display one new singlet signal, at around δ 3.05 ppm, attributed to the C$_c$–CH_2–styrenyl protons.[12a] Besides, other resonances attributed to the benzyl group protons are observed in the range 7.34–6.88 ppm, and the vinyl group in the range 6.82–5.31 ppm (see ESI†).

The ^{11}B{^{1}H} NMR spectra for **3–4** show the typical, 2 : 6 : 2 and 2 : 5 : 1 : 1 : 1 pattern,[17a] respectively. As for previously reported iodinated carboranes,[17,22] the *B*–I is identified as the highest field resonances at −23.96 ppm, which remains as a singlet in the ^{11}B{^{1}H} NMR. The ^{11}B{^{1}H} NMR spectra of **5–6** show overlapped boron resonances with patterns 16 : 64 or 16 : 40 : 16 : 8, respectively. The ^{13}C{^{1}H} NMR spectra of **3–4** show the aromatic resonances in the range 137–124 ppm and two signals attributed to C$_c$–*C*H$_2$ carbons at around δ = 33 and 42 ppm. Two other additional resonances corresponding to the vinyl group appear in the range δ = 136 and 114 ppm. Moreover, the ^{13}C{^{1}H} NMR spectra of **5–6** show the aromatic and alkene resonances between 149 and 117 ppm, whereas peaks in the region 77–75 ppm are attributed to the *C*$_c$–C. The methylene groups resonances appear in the range δ 42–33 ppm.

Finally, transmission electron microscopy (TEM) images of the octavinylsilsesquioxane (OVS) and **5–6** have been obtained (see Fig. 1) and some important differences in the morphology of the particles have been observed. The starting OVS forms cubic-like particles, whereas **5–6** have a spherical shape with a broad particle-size distribution. The shape of these spherical particles obtained for **5–6** is very similar to previous reported *o*-carboranyl–styrene decorated octasilsesquioxanes,[18] but with

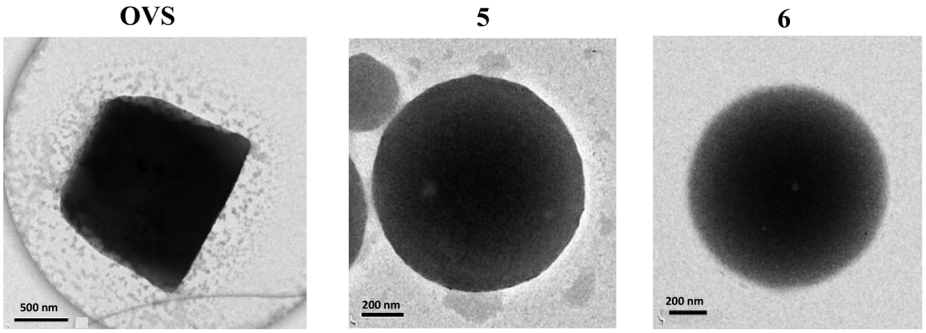

Fig. 1 TEM photographs of the octavinylsilsesquioxane (OVS) and **5–6**.

a higher size, which suggests that the presence of the anthracenyl does not affect the shape of the hybrid.

X-ray structural analysis

Single-crystals of **3** suitable for X-ray structural determination were obtained by slow evaporation from a mixture of chloroform/*n*-heptane (9 : 1) at room temperature. The molecular structure for **3** was established by single-crystal X-ray diffraction (Fig. 2) and agree with the NMR data (*vide supra*). Experimental crystal data and structure refinement parameters for the structure are listed in Table 1. The triad **3** crystallizes in the monoclinic system $P2_1/c$ space group. The molecular structure shows a typical icosahedral geometry with similar bond distances and angles to those *m*-carborane–anthracene dyads and triads previously reported.[17]

In the structure of **3**, the *m*-carborane moiety is linked from the C_c to one anthracene unit through a methylene spacer ($-CH_2-$), and likewise from the adjoining C_c to one styrene unit. As shown in Fig. 2, the rotation of the anthracene and benzene rings through the (H)(H)C–C(anthracene–benzene) bond allows more or less similar conformations in the solid-state. Conformations found in the solid-state and torsion angles can be seen in Fig. 2 caption.

The solid-state structure in **3** is dominated by intermolecular C–H···π interactions (Fig. S1† and Table 2), mainly between (H)C–H···$C_{anthracene}$ (Fig. S1† and Table 2). Moreover, interactions between $-CH_2-$ hydrogens and vinyl carbons are found. Other weak B–H···H–C contact is listed in Table 2. From the crystal packing of **3** (Fig. 2, Fig. S1†), we may determine that there are not π–π stacking between two anthracenes or between anthracene and benzene units, due to the presence of the $-CH_2-$ spacer, from which one hydrogen atom interacts with an aromatic $C_{anthracene}$ (~2.9 Å) avoiding the intermolecular π–π interactions.

From the fingerprint plots analysis, it immediately emerges that H···H contacts comprise nearly 72% of the total Hirshfeld surface area for compound **3**. The H···C contacts contribute around 28% to the total Hirshfeld surface area, whereas the contribution of C···C contacts (*e.g.*, π···π interactions) is less than 1% (see more details in ESI†).

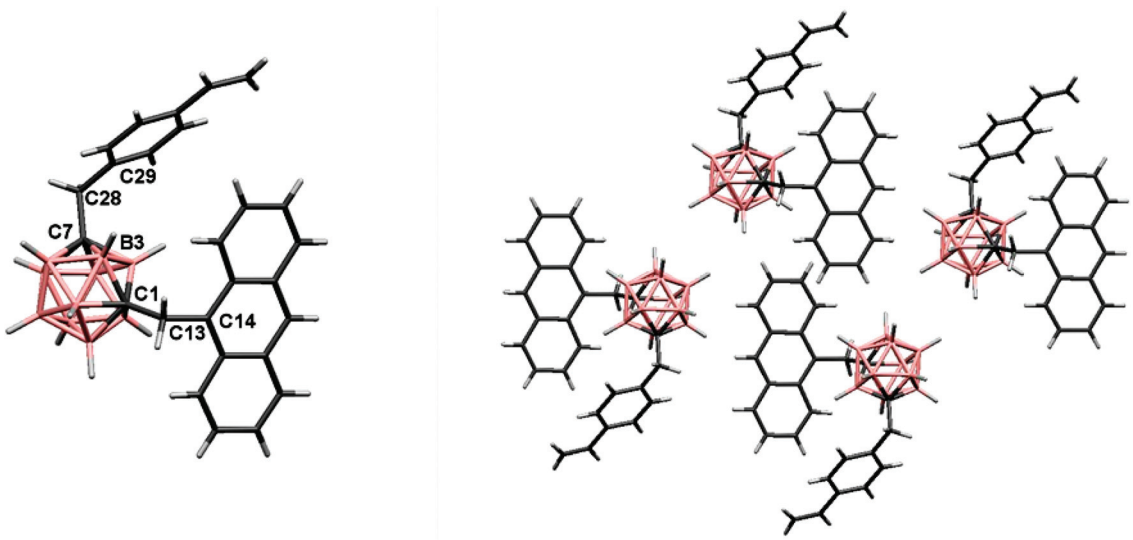

Fig. 2 (Left) Molecular structure of **3**. Torsion angles: $C_{29}C_{28}C_7B_3$, −40.4(2)° and $C_{14}C_{13}C_1B_3$, −38.3(2)°; (right) projections showing the organization of four molecules of **3** in the solid-state. Color code: B pink; C grey; H white.

Table 1 Crystal data and refinement details for the structure of **3**

	3
Empirical formula	$C_{26}H_{30}B_{10}$
Formula weight	450.60
Crystal system	Monoclinic
Space group	$P2_1/c$
Temperature/K	293(2)
Wavelength/Å	0.71073
a/Å	10.3008(18)
b/Å	11.295(3)
c/Å	22.279(4)
α/°	90
β/°	97.941(7)
γ/°	90
Volume/Å^3	2567.3(9)
Z	4
Density (calculated)/Mg m^{-3}	1.166
F(000)	944
Theta range for data collection/°	2.581 to 27.484
Absorption coefficient/mm^{-1}	0.060
Goodness-of-fit on F^2	1.029
R_1 [I > 2sigma(I)]	0.0524
wR_2 [I > 2sigma(I)]	0.1287
R_1 (all data)	0.0710
wR_2 (all data)	0.1405

CCDC 1972767 (**3**) contain the supplementary crystallographic data for this paper.†

Table 2 Geometrical parameters of weak D–H···A (A = C, H) contacts (Å, °), involved in the supramolecular construction in **3**

Compound	D–H···A	d(H···A)	<(DHA)	<(HHB)
3	C(13)–H(13B)···C(23)^{i}	2.892	168.27	
	C(13)–H(13A)···C(34)^{ii}	2.977	150.4	
	C(28)–H(28B)···C(21)^{iii}	2.937	171	
	C(28)–H(28A)···H(4)–B(4)^{iv}	2.437	123.2	109.31

Symmetry codes (i) $-x$, $1/2 + y$, $3/2 - z$ (ii) x, $3/2 - y$, $1/2 + z$ (iii) $1 - x$, $1/2 + y$, $3/2 - z$ (iv) $1 - x$, $1/2 + y$, $3/2 - z$.

Photophysical properties and TD-DFT calculations

The photophysical properties of **3–6** were determined by UV-Vis absorption and fluorescence spectroscopies in THF, as well as in a mixture of THF/water (v/v = 1/99) to form aggregates (Table 3). Electronic properties of **3–6** in the ground state were assessed by UV-Vis absorption measurements (~10^{-5} M for **3–4** and ~10^{-6} M for **5–6**, Fig. 3). All compounds exhibit similar absorption spectra with vibrational structures and the four characteristic peaks at around 334, 351, 369 and 389 nm assigned to the π–π^* transition band of the anthracene moiety, as was previously observed for precursors **1–2**.[17] This suggests that the incorporation of the methyl–styrenyl group through the neighboring C_c does not alter the absorption patterns of the anthracene. The molar extinction coefficients (ε) are significantly different between monomers **3–4** and hybrids **5–6**. For **3–4** the ε values were in the range from 94×10^2 to 99×10^2 M^{-1} cm^{-1}, slightly lower than their precursors **1–2** (102×10^2 and 106×10^2 M^{-1} cm^{-1}, respectively);[17b] whereas for **5–6** higher values in the range from 553×10^2 to 630×10^2 M^{-1} cm^{-1} were obtained. The molar extinction coefficients for the carboranyl-containing POSS hybrids are almost six times larger than the values found for the individual precursors (**3–4**), so that the ratio of absorption per carboranyl triad is higher when this unit is attached to the POSS cage, which assembles eight fluorophores per molecule (Table 3).

Photoluminescence emission spectra of **3–6** were also measured in THF. All of them show similar vibronic emission spectra in solution, with maxima around λ_{em} = 415 nm (Fig. 3a), that can be assigned to the locally excited estate (LE) emission of the anthracene moiety. The similarity between spectra of **3–4** in solution to the one from anthracene itself (λ_{em} = 420 nm) suggests that only small electronic interactions between anthracene units take place, and there is no electronic or steric influence of the iodo or styrene groups, which is in full agreement with the DFT calculations (*vide infra*). This is proven because **3–4** exhibit fluorescence quantum yield values (ϕ_F) near 100% in solution, that is comparable to the ϕ_F of precursors **1–2**,[17b] demonstrating that the fluorescence efficiency is mostly given by the anthracene/carboranyl group, whereas the influence of the styrene is negligible. Moreover, these results are consistent with previous reports,[15–17] where *m*-carborane bound to other fluorophores produced an important increase of the quantum efficiency.

Moreover, when triads **3–4** were grafted to the OVS cube structure, the quantum yields drop to 34–45% for **5–6** in solution. If we compare these values with others reported for similar structures bearing *o*-carborane, Me-*o*-carborane and Ph-*o*-carborane, with ϕ_F 0.02, 0.09 and 0.44, respectively,[18] we may conclude that the synergistic combination of the anthracene luminophore with the *m*-carborare, which is a less electron-acceptor group that the *o*-carborane, results in higher

Table 3 Photophysical data for compounds **3–6**

	THF					THF/water (1/99)			
Compounds	λ_{abs} (nm)	$\varepsilon/10^5$ (M^{-1} cm^{-1})	λ_{em} (nm)	ϕ_F [a]	Stokes shift (nm)	λ_{abs} (nm)	λ_{em} (nm)	ϕ_F [a]	Stokes shift (nm)
3	369	0.099	414	1	45	371	457	0.31	86
4	369	0.094	415	0.98	46	373	455	0.26	82
5	369	0.553	415	0.34	46	373	457	0.36	84
6	369	0.630	416	0.45	47	373	456	0.27	83

[a] Reference compound quinine sulfate (0.5 M H_2SO_4, ϕ_F = 0.54).

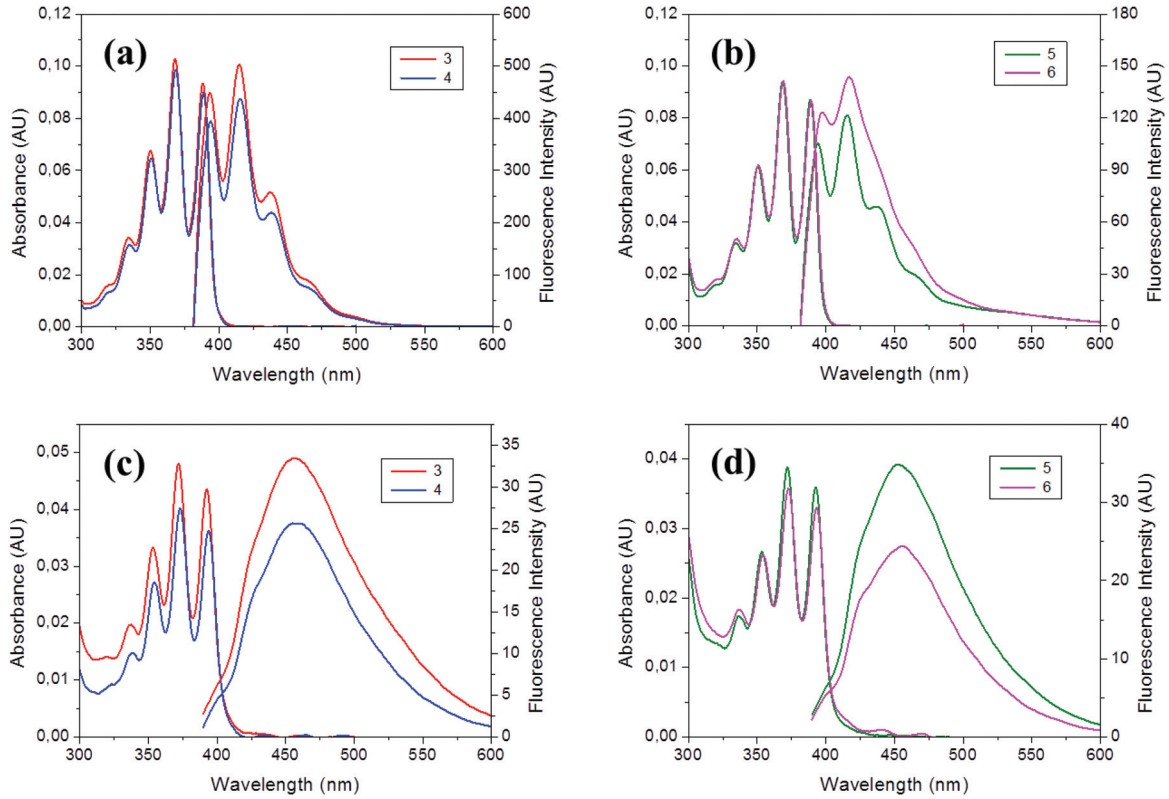

Fig. 3 Absorption and emission spectra of **3–6** in THF solutions (a–b) and aggregates (THF/H_2O, v/v = 1/99) (c–d). AU: arbitrary units.

luminescent POSS hybrids. Table 3 summarizes the photophysical data for all the compounds.

Finally, we investigated the PL behavior in the aggregate state (THF/H_2O = 1/99 (v/v), 1×10^{-5} M for **3–4** and 1×10^{-6} M for **5–6**). The PL spectra for these compounds are very similar, showing non-vibronic structures and a maximum emission around 455–459 nm (Table 3 and Fig. 3c and d), red-shifted about 40 nm, with regard to the THF solutions. Consequently, larger Stokes shifts are also observed. Noticeably, similar moderate fluorescence quantum yields were determined for hybrids **5–6** (ϕ_F = 27–36%) and monomers **3–4** (26–31%), suggesting that neither the free monomers nor the hybrids obtained after their coupling to OVS have π–π interactions in solid-state, as it was discussed above for the crystal packing of **3**. Nevertheless, a significant drop of the fluorescence efficiency occurs in aggregates **3–4** (26–31%) with regard to the solution (98–100%), probably due to the restriction of the rotation of the anthracene units.

To get a better insight into the nature of the photophysical properties of the investigated compounds, DFT calculations were performed (more details in ESI†). Several rotamers were considered and between the rotamers, the energy differences are small (Fig. S2 in the ESI†). In the case of **3**, the structure obtained from the single-crystal X-ray diffraction was optimized at ω-B97XD/6-31+G* level not showing any significant difference from the structure from X-ray diffraction. As can be expected this structure exhibits the highest stability among the investigated rotamers (ΔE = 4.0–5.1 kcal mol^{-1} at ω-B97XD/6-31G* level of theory, Fig. S2†). Investigating the Kohn–Sahm frontier orbitals of the different rotamers it can be established that, the energy ($\Delta\varepsilon$ < 0.2 eV) and the shape of the orbitals does not depend strongly on the orientation of the substituents in agreement with the small energy differences between the rotamers. In the case of **3** both the HOMO and LUMO are localized at the anthracene unit (Fig. 4 and Fig. S3†), but the orbitals of the styrenyl moiety also appear in the frontier orbital region (HOMO−1, LUMO+1, see Fig. 4 and Fig. S3†). The π-systems of anthracene and styrene units do not interact with each other and the energy of the above-mentioned orbitals are very close to the energy of the corresponding orbitals of the parent anthracenyl-*m*-carborane (**1**) and stirenyl-*m*-carborane (Fig. 4); this further supports the lack of interaction between them. In the case of **4** the shape and energy level of HOMO and LUMO are similar to **3** and the lone pairs of the iodine atoms appear as HOMO−2 and HOMO−3 (Fig. S3†).

TD-DFT calculations were performed at different level of theory. The geometry was obtained at ω-B97XD/6-31+G* level of theory and this geometry was used for the further TD-DFT calculations. Several methods and basis sets were tested (Table S1 in ESI†) and, in agreement with our previous results,[17,23] the B3LYP method with the rather small 6-31G basis set gives the best numerical results, only 5 nm error for both **3** and **4** (calculated: 384 nm *vs.* experimental: 389 nm, note that simple TD-DFT calculations could not interpret the

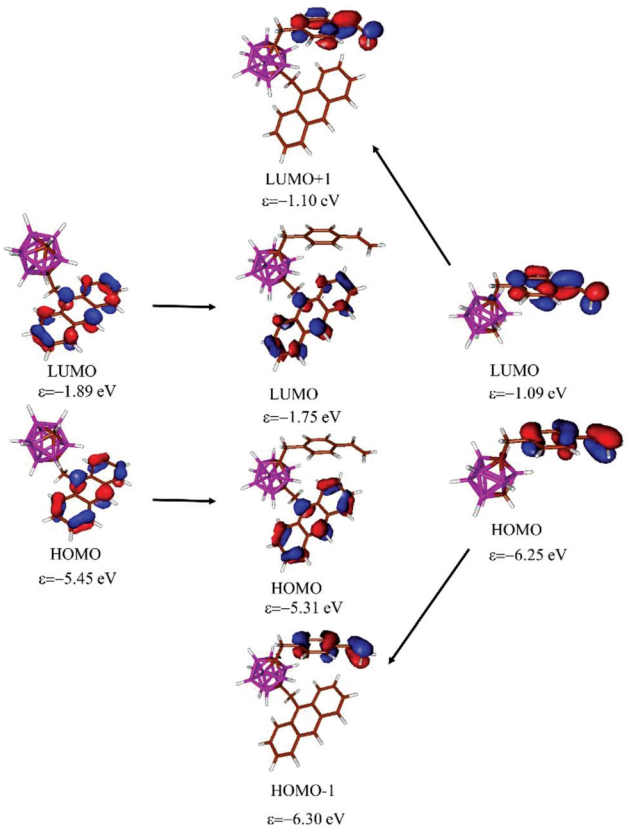

Fig. 4 Kohn–Sahm molecular orbitals of anthacenyl-*m*-carborane **1** (left), **3** (middle) and styrenyl-*m*-carborane (right) at B3LYP/6-31G*// ω-B97XD/6-31+G* level of theory.

vibrational fine structure, which is unique for rigid aromatic system such as anthracene). These results confirmed that the transition corresponds to the local π–π* (HOMO–LUMO) transition of the anthracene moiety.

For **4**, it should be noted that the lone pairs of the iodo atoms are in the border orbitals' region (HOMO−2, HOMO−3 in the ESI†). Moreover, TD-DFT calculations show transitions from these orbitals to the LUMO (fifth and sixth excited states, see in Table S3†), and the calculated oscillator strength (which corresponds to the intensity of the peaks in the experimental spectra) of these transitions are low (<0.002), thus they could not be observed experimentally. Therefore, the presence of iodo groups does not affect the photophysical properties of the parent compound.

The geometry optimization of **5** and the TD-DFT calculations were performed as well (more details in Table S4†); they gave questionable geometry and overestimated the absorption peak by 30 nm (it should be highlighted that these systems are quite huge for simple DFT calculations (more than 500 atoms)). To obtain a better description of the effect of the octasilsesquioxane substitutions, one of its arms (trimethoxysilyl substituted derivatives see Fig. S4 in the ESI†) was calculated. As it can be expected the substitution at the styrenyl unit does not affect the shape and the energy of the frontier orbitals (localised at the anthracene unit, Fig. S4†), which is in agreement with the experimentally observed spectra.

Conclusions

A set of two new C-heterosubstituted *m*-carborane triads bearing one anthracene and one styrene group (**3–4**) along with octasilsesquioxane-based hybrids (**5–6**) decorated with eight of those triads have been successfully synthesized, isolated and fully characterized. TEM images of OVS and **5–6** show important differences in the morphology of the particles; whereas OVS forms cubic-like particles, **5–6** have spherical shapes with a broad particle-size distribution. The crystal structure of **3** was analyzed by X-ray diffraction. According to their emission spectra, all compounds show similar vibronic emissions in solution assigned to the locally excited estate (LE) emission of the anthracene moiety. The similarity between these spectra to the anthracene itself suggested that only small electronic interactions between the anthracene units occurred, as it was confirmed by TD-DFT calculations. The calculated oscillator strengths corresponding to the transitions from iodo orbitals to the LUMO were low and could not be observed experimentally. Thus, the presence of iodo units did not affect the photophysical properties of our systems. On the other hand, due to its large dimension for simple DFT calculations, only one arm of **5** and **6** has been calculated as a model system, suggesting that the substitution at the styrenyl unit did not affect the shape and the energy of the frontier orbitals. Extraordinary fluorescence efficiencies, around the unity, were exhibited for triads **3–4** in solution, being lower for hybrids **5–6**. Noticeably, all of them exhibited quite high fluorescence quantum yield values in the aggregate state. In agreement with earlier scattered data on *m*-carborane related to other fluorofores, herein we provide extra results that evidence that *m*-carborane is a suitable scaffold for coupling to anthracene to produce excellent emitters in solution, while maintaining the emission properties in the aggregate state. The ϕ_F on anthracene has increased to near 100% upon the linkage to the *m*-carborane. An explanation that is consistent with the experimental and computational details is that *m*-carborane does not alter the energy levels participating in the fluorescence, mainly due to anthracene, however it prevents alternative non-radiative transitions. DFT and TDDFT calculations have given support to the non-influence of *m*-carborane in the orbitals participating in the PL, but have not provided any hint for the high quantum yield. Taking into account the potential of *m*-carborane based fluorophores, in the future we plan to explore other related compounds and carry out calculations at higher level of theory (*e.g.* CASPT2) that require much more computational time and do molecular dynamic calculations (MD) that may give more precise information. In addition, we will focus in exploiting and studying the potential applications of *m*-carborane-containing fluorophores.

Experimental

Instrumentation

Elemental analyses were performed using a Carlo Erba EA1108 microanalyzer. ATR-IR spectra were recorded on JASCO FT/IR-4700 spectrometer on a high-resolution. The ^{1}H NMR (300.13 MHz), ^{11}B{^{1}H} (96.29 MHz) and ^{13}C{^{1}H} NMR (75.47 MHz) spectra were recorded on a Bruker ARX 300 spectrometer. All NMR spectra were recorded in $CDCl_3$ solutions at 25 °C. Chemical shift values for ^{11}B {^{1}H} NMR spectra were referenced to external $BF_3{\cdot}OEt_2$, and those for ^{1}H and ^{13}C {^{1}H} NMR were referenced to $SiMe_4$ (TMS). Chemical shifts are reported in units of parts per million downfield from the reference, and all coupling constants are reported in Hertz. UV-Vis spectra were recorded on VARIANT Cary 5 UV-Vis-NIR spectrophotometer, using spectroscopic grade THF (Sigma-Aldrich), in normal quartz cuvette having 1 cm path length, for different solutions for each compound in the range 5×10^{-5} to 1×10^{-5} M to calculate the molar extinction coefficients (ε). The fluorescence emission spectra and excitation spectra for all samples were recorded in a VARIANT Cary Eclipse Fluorescence spectrometer. No fluorescent contaminants were detected on excitation in the wavelength region of experimental interest. The fluorescence quantum yields were determined by the "single point method" and repeated three times with similar optical density for reproducibility,[24] against quinine sulfate in 0.5 M aqueous sulfuric acid with $\phi_F = 0.54$ as a standard.[25] For the suspensions in THF/water (1/99, v/v) the refractive index was assumed to be that of pure water (1.33).

Materials

All reactions were performed under an atmosphere of dinitrogen employing standard Schlenk techniques. Tetrahydrofuran and dichloromethane were purchased from Merck and distilled from sodium benzophenone before to use. Commercial grade diethyl ether, hexane, petroleum ether, *n*-heptane, and chloroform were used without further purification. Compounds **1–2** were synthesized according to the literature.[17b] *n*-BuLi solution (1.6 M in hexane), Grubbs 1st generation catalyst [$RuCl_2$(CHPh)-(PCy_3)2], Octavinylsilsesquioxane (OVS) were purchased from Aldrich. 4-Vinylbenzyl chloride was purchased from ACROS Organics.

X-ray single-crystal structure determination

The crystal structure of compound **3** was determined by single-crystal X-ray crystallography. A suitable crystal of this material was mounted on a MITEGEN Micro mount™ and used for the data collection on a Bruker D8 Venture diffractometer using MoKα radiation (λ = 0.71073 Å). Absorption correction was applied using SADABS.[26] The structure was solved by direct methods which revealed the position of all non-hydrogen atoms and refined with full-matrix least-squares calculations on F^2,[27] using Olex2 as the graphical interface.[28] Anisotropic displacement parameters were assigned to all atoms except for hydrogen atoms, which are riding their parent atoms with an isotropic temperature factor chosen as 1.2 times those of their parent atoms. Details of the structure determination and refinement of the studied compounds are summarized in Table 1. Crystallographic data for the structure reported in this paper have been deposited in the Cambridge Crystallographic Data Centre, CCDC 1972767.†

Synthesis of 3. A 1.6 M solution of *n*BuLi in hexane (0.68 mL, 1.088 mmol) was added dropwise to a solution of **1** (315 mg, 0.942 mmol) in THF (10 mL) at 0 °C. The mixture was stirred for 1 h at room temperature, cooled to 0 °C, and 4-vinylbenzyl chloride (0.17 mL, 1.090 mmol) was added. The mixture was stirred and refluxed at 75 °C overnight, after which the solvent was removed under vacuum and the mixture was quenched with H_2O (10 mL), transferred to a separating funnel, and extracted with Et_2O (3 × 10 mL). The organic layer was dried with $MgSO_4$ and the volatile substances were removed under vacuum. The yellowish oil was purified by preparative layer chromatography (hexane) to give to give **3** as a yellowish solid. Yield: 0.259 g, 61%. Crystals suitable for X-ray analysis were obtained by slow evaporation of a solution of **3** in chloroform/*n*-heptane. ^{1}H NMR, δ (ppm): 8.44 (s, 1H, $C_{14}H_9$), 8.12 (d, ^{3}J(H,H) = 9 Hz, 2H, $C_{14}H_9$), 8.03 (d, ^{3}J(H,H) = 9 Hz, 2H, $C_{14}H_9$), 7.58–7.54 (m, 2H, $C_{14}H_9$), 7.53–7.49 (m, 2H, $C_{14}H_9$), 7.33 (d, ^{3}J(H,H) = 6 Hz, 2H, C_6H_4), 6.94 (d, ^{3}J(H,H) = 9 Hz, 2H; C_6H_4), 6.77 (dd, ^{3}J(H,H) = 18 Hz, ^{3}J(H,H) = 12 Hz, 1H, C*H*═CH_2), 5.83 (d, ^{3}J(H,H) = 18 Hz, 1H, CH═CH_2), 5.35 (d, ^{3}J(H,H) = 12 Hz, 1H, CH═CH_2), 4.22 (s, 2H, CH_2–$C_{14}H_9$), 3.06 (s, 2H, CH_2–C_6H_4); ^{1}H{^{11}B} NMR, δ (ppm): 8.44 (s, 1H, $C_{14}H_9$), 8.12 (d, ^{3}J(H,H) = 9 Hz, 2H, $C_{14}H_9$), 8.03 (d, ^{3}J(H,H) = 9 Hz, 2H, $C_{14}H_9$), 7.58–7.54 (m, 2H, $C_{14}H_9$), 7.53–7.49 (m, 2H, $C_{14}H_9$), 7.33 (d, ^{3}J(H,H) = 6 Hz, 2H, C_6H_4), 6.94 (d, ^{3}J(H,H) = 9 Hz, 2H; C_6H_4), 6.77 (dd, ^{3}J(H,H) = 18 Hz, ^{3}J(H,H) = 12 Hz, 1H, C*H*═CH_2), 5.83 (d, ^{3}J(H,H) = 18 Hz, 1H, CH═CH_2), 5.35 (d, ^{3}J(H,H) = 12 Hz, 1H, CH═CH_2), 4.22 (s, 2H, CH_2–$C_{14}H_9$), 3.06 (s, 2H, CH_2–C_6H_4), 2.61 (s, 1H, B–*H*), 2.51 (s, 2H, B–*H*), 2.28 (s, 3H, B–*H*), 2.18 (s, 2H, B–*H*), 2.14 (s, 2H, B–*H*); ^{11}B{^{1}H} NMR, δ (ppm): −6.61 (s, 2B), −11.09 (s, 6B), −13.61 (s, 2B); ^{13}C{^{1}H} NMR, δ (ppm): 136.80 (s, C_6H_4), 136.51 (s, *C*H═CH_2), 131.40 (s, $C_{14}H_9$), 130.82 (s, $C_{14}H_9$), 130.03 (s, C_6H_4), 129.49 (s, $C_{14}H_9$), 129.25 (s, $C_{14}H_9$), 128.19 (s, $C_{14}H_9$), 126.23 (s, $C_{14}H_9$ and C_6H_{14}), 124.99 (s, $C_{14}H_9$), 124.78 (s, $C_{14}H_9$), 114.06 (s, CH═*C*H_2), 76.30 (s, C_c–CH_2), 75.84 (s, C_c–CH_2), 42.70 (s, *C*H_2–C_6H_4), 33.77 (s, *C*H_2–$C_{14}H_9$); ATR-IR (cm^{-1}): ν = 3052, 2927, 2853 (C_{ar}–H), 2596, 2587, 2572, 2557 (B–H), 1624 (C═C); elemental analysis calcd (%) for $C_{26}H_{30}B_{10}$: C, 69.30; H, 6.71. Found: C, 68.80; H, 6.74.

Synthesis of 4. The procedure was the same as for **3**, but using a solution of **2** (0.378 g, 0.821 mmol) in THF (10 mL), *n*BuLi 1.6 M in hexanes (0.59 mL, 0.944 mmol) and a solution of 4-vinylbenzyl chloride (0.15 mL, 0.962 mmol). After extraction with 3 × 10 mL of brine/Et_2O, the yellowish oil residue was purified by preparative layer chromatography (petroleum ether) to give **4** as yellowish solid. Yield: 0.317 g, 67%. ^{1}H NMR, δ (ppm): 8.45 (s, 1H, $C_{14}H_9$), 8.04 (t, ^{3}J(H,H) = 7.5 Hz, 4H, $C_{14}H_9$), 7.57–7.48 (m, 4H, $C_{14}H_9$), 7.30 (d, ^{3}J(H,H) = 9 Hz, 2H, C_6H_4), 6.89 (d, ^{3}J(H,H) = 9 Hz, 2H; C_6H_4), 6.74 (dd, ^{3}J(H,H)

= 18 Hz, ^3J(H,H) = 12 Hz, 1H, C*H*=CH$_2$), 5.80 (d, ^3J(H,H) = 18 Hz, 1H, CH=C*H*$_2$), 5.33 (d, ^3J(H,H) = 12 Hz, 1H, CH=C*H*$_2$), 4.24 (s, 2H, C*H*$_2$–C$_{14}$H$_9$), 3.05 (s, 2H, C*H*$_2$–C$_6$H$_4$); ^{11}B{^{1}H} NMR, δ (ppm): −5.60 (s, 2B), −10.04 (s, 5B), −13.56 (s, 1B), −15.48 (s, 1B), −23.96 (s, 1B); ^{13}C{^{1}H} NMR, δ (ppm): 137.01 (s, *C*$_6$H$_4$), 136.33 (s, *C*H=CH$_2$), 135.79 (s, *C*$_6$H$_4$), 131.34 (s, *C*$_{14}$H$_9$), 130.67 (s, *C*$_{14}$H$_9$), 129.88 (s, C$_6$H$_4$), 129.30 (s, *C*$_{14}$H$_9$), 128.73 (s, *C*$_{14}$H$_9$), 128.42 (s, *C*$_{14}$H$_9$), 126.41 (s, *C*$_{14}$H$_9$), 126.32 (s, *C*$_6$H$_4$), 125.02 (s, *C*$_{14}$H$_9$), 124.37 (s, *C*$_{14}$H$_9$), 114.24 (s, CH=*C*H$_2$), 42.49 (s, *C*H$_2$–C$_6$H$_4$), 33.60 (s, *C*H$_2$–C$_{14}$H$_9$); ATR-IR (cm^{-1}): ν = 3083, 3035, 2927, 2852 (C$_{ar}$–H), 2593 (B–H), 1623 (C=C); elemental analysis calcd (%) for C$_{26}$H$_{29}$B$_{10}$I: C, 54.17; H, 5.07. Found: C, 54.10; H, 5.07.

Synthesis of 5. A 10 mL round-bottomed flask was charged under nitrogen with OVS (15 mg, 0.024 mmol), compound **3** (102.5 mg, 0.227 mmol), and first generation Grubbs catalyst (12 mg, 0.014 mmol) in 5 mL of CH_2Cl_2. The solution was stirred and refluxed at 40 °C for three days. The solvent was removed under vacuum. The residue was treated with a mixture of THF/MeOH (1 : 10) to obtain a grey solid. Further purification was performed by preparative layer chromatography (CH_2Cl_2/hexane, 7 : 3) to obtain compound **5** as yellowish solid. Yield: 49 mg, 52%. ^{1}H NMR, δ (ppm): 8.28 (s, 8H, C$_{14}$*H*$_9$), 7.97 (d, ^3J(H,H) = 10 Hz, 16H, C$_{14}$*H*$_9$), 7.89 (d, ^3J(H,H) = 8 Hz, 16H, C$_{14}$*H*$_9$), 7.54 (d, ^3J(H,H) = 18 Hz, 8H, C*H*=CH–Si), 7.46–7.40 (m, 48H, C$_6$*H*$_4$ and C$_{14}$*H*$_9$), 6.91 (d, ^3J(H,H) = 8 Hz, 16H, C$_6$*H*$_4$), 6.51 (d, ^3J(H,H) = 20 Hz, 8H, CH=*C*H–Si), 4.04 (s, 16H, C*H*$_2$–C$_{14}$H$_9$), 3.00 (s, 16H, C*H*$_2$–C$_6$H$_4$); ^{11}B{^{1}H} NMR, δ (ppm): −6.52 (br, 16B), −10.81 (br, 48B), −13.33 (br, 16B); ^{13}C{^{1}H} NMR, δ (ppm): 148.68 (s, *C*H=CH–Si), 137.54 (s, *C*$_6$H$_4$), 136.10 (s, *C*$_6$H$_4$), 130.94 (s, *C*$_{14}$H$_9$), 130.36 (s, *C*$_{14}$H$_9$), 129.86 (s, *C*$_6$H$_4$), 129.03 (s, *C*$_6$H$_4$), 128.88 (s, *C*$_{14}$H$_9$), 127.79 (s, *C*$_6$H$_4$), 126.70 (s, *C*$_{14}$H$_9$), 125.85 (s, *C*$_{14}$H$_9$), 124.61 (s, *C*$_{14}$H$_9$), 124.33 (s, *C*$_{14}$H$_9$), 117.23 (s, CH=*C*H–Si), 75.94 (s, *C*$_c$–CH$_2$), 75.17 (s, *C*$_c$–CH$_2$), 42.32 (s, *C*H$_2$–C$_6$H$_4$), 33.29 (s, *C*H$_2$–C$_{14}$H$_9$); ^{29}Si NMR ($CDCl_3$): δ = −78.09; ATR-IR (cm^{-1}): $\tilde{\nu}$ = 3034, 2957, 2929, 2867 (C$_{ar}$–H), 2589 (B–H), 1605 (C=C), 1087 (Si–O); elemental analysis calcd (%) for C$_{208}$H$_{232}$B$_{80}$O$_{12}$Si$_8$ + 2 C$_6$H$_{14}$: C, 63.12; H, 6.26. Found: C, 63.18; H, 6.07.

Synthesis of 6. The procedure was the same as for **5**, but using a solution of OVS (15 mg, 0.024 mmol), compound **4** (131.1 mg, 0.227 mmol), and first generation Grubbs catalyst (12 mg, 0.014 mmol) in 5 mL of CH_2Cl_2. After workup, **6** was obtained as a yellowish solid. Yield: 60 mg, 50%. ^{1}H NMR, δ (ppm): 8.30 (s, 8H, C$_{14}$*H*$_9$), 7.91 (d, ^3J(H,H) = 10 Hz, 32H, C$_{14}$*H*$_9$), 7.52 (d, ^3J(H,H) = 20 Hz, 8H, C*H*=CH–Si), 7.46–7.38 (m, 48H, C$_6$*H*$_4$ and C$_{14}$*H*$_9$), 6.87 (d, ^3J(H,H) = 8 Hz, 16H, C$_6$*H*$_4$), 6.50 (d, ^3J(H,H) = 20 Hz, 8H, CH=*C*H–Si), 4.04 (s, 16H, C*H*$_2$–C$_{14}$H$_9$), 3.00 (s, 16H, C*H*$_2$–C$_6$H$_4$); ^{11}B{^{1}H} NMR, δ (ppm): −5.35 (br, 16B), −9.36 (br, 40B), −14.97 (br, 16B), −23.64 (br, 8B); ^{13}C{^{1}H} NMR, δ (ppm): 148.57 (s, *C*H=CH–Si), 136.96 (s, *C*$_6$H$_4$), 136.28 (s, *C*$_6$H$_4$), 130.93 (s, *C*$_{14}$H$_9$), 130.27 (s, *C*$_{14}$H$_9$), 129.77 (s, *C*$_6$H$_4$), 129.00 (s, *C*$_6$H$_4$), 128.32 (s, *C*$_{14}$H$_9$), 128.09 (s, *C*$_6$H$_4$), 126.81 (s, *C*$_{14}$H$_9$), 126.12 (s, *C*$_{14}$H$_9$), 124.72 (s, *C*$_{14}$H$_9$), 123.98 (s, *C*$_{14}$H$_9$), 117.43 (s, CH=*C*H–Si), 77.17 (s, *C*$_c$–CH$_2$), 76.52 (s, *C*$_c$–CH$_2$), 42.10 (s, *C*H$_2$–C$_6$H$_4$), 33.14 (s, *C*H$_2$–C$_{14}$H$_9$); ^{29}Si NMR ($CDCl_3$): δ = −78.15; ATR-IR (cm^{-1}): $\tilde{\nu}$ = 2955, 2922, 2851 (C$_{ar}$–H), 2593 (B–H), 1604 (C=C), 1085 (Si–O); elemental analysis calcd (%) for C$_{208}$H$_{224}$B$_{80}$I$_8$O$_{12}$Si$_8$ + 2 C$_6$H$_{14}$ + CH_2Cl_2: C, 50.29; H, 4.85. Found: C, 50.30; H, 5.09.

Conflicts of interest

The authors declare no conflict of interest.

Acknowledgements

The work was supported by Spanish Ministerio de Economía y Competitividad, MINEICO (CTQ2016-75150-R and "Severo Ochoa" Program for Centers of Excellence in R&D SEV-2015-0496) and Generalitat de Catalunya (2017/SGR/1720). Z. K. is grateful for the general support of the European Union's Horizon 2020 research and innovation program under the Marie Skłodowska-Curie grant agreement MSCA-IF-2016-751587. D. Ch.-L. acknowledges funding by project No. PGC2018-102047-B-I00 (MCIU/AEI/FEDER, UE). Theoretical calculations have been achieved using computers from the Supercomputing Centre of Catalonia (CESCA).

References

1 (*a*) H. Nakanotani, T. Higuchi, T. Furukawa, K. Masui, K. Morimoto, M. Numata, H. Tanaka, Y. Sagara, T. Yasuda and C. Adachi, High-efficiency organic light-emitting diodes with fluorescent emitters, *Nat. Commun.*, 2014, **5**, 4016; (*b*) H. Xu, R. F. Chen, Q. Sun, W. Y. Lai, Q. Q. Su, W. Huang and X. G. Liu, Recent progress in metal–organic complexes for optoelectronic applications, *Chem. Soc. Rev.*, 2014, **43**, 3259–3302; (*c*) O. Ostroverkhova, Organic Optoelectronic Materials: Mechanisms and Applications, *Chem. Rev.*, 2016, **116**, 13279–13412; (*d*) Z. Yang, Z. Mao, Z. Xie, Y. Zhang, S. Liu, J. Zhao, J. Xu, Z. Chi and M. P. Aldred, Recent advances in organic thermally activated delayed fluorescence materials, *Chem. Soc. Rev.*, 2017, **46**, 915–1016; (*e*) H. Dong, C. Zhang, X. Lin, Z. Zhou, J. Yao and Y. S. Zhao, Dual-Wavelength Switchable Vibronic Lasing in Single-Crystal Organic Microdisks, *Nano Lett.*, 2017, **17**, 91–96.

2 (*a*) Q. Ye, H. Zhou and J. Xu, Cubic Polyhedral Oligomeric Silsesquioxane Based Functional Materials: Synthesis, Assembly, and Applications, *Chem. – Asian J.*, 2016, **11**, 1322–1337; (*b*) R. M. Laine and M. F. Roll, Polyhedral Phenylsilsesquioxanes, *Macromolecules*, 2011, **44**(55), 1073–1109; (*c*) S. Sulaiman, J. Zhang III, T. Goodson and R. M. Laine, Synthesis, characterization and photophysical properties of polyfunctional phenylsilsesquioxanes: [o-RPhSiO$_{1.5}$]$_8$, [2,5-R$_2$PhSiO$_{1.5}$]$_8$, and [R$_3$PhSiO$_{1.5}$]$_8$. Compounds with the highest number of functional units/unit volume, *J. Mater. Chem.*, 2011, **21**, 11177–11187; (*d*) D. B. Cordes, P. D. Lickiss and F. Rataboul, Recent

Developments in the Chemistry of Cubic Polyhedral Oligosilsesquioxane, *Chem. Rev.*, 2010, **110**, 2081–2173.

3 C. Hartmann-Thompson, *Applications of Polyhedral Oligomeric Silsesquioxanes*, Springer, Netherlands, Midland, 2011, vol. 3.

4 (*a*) T. Maegawa, O. Miyashita, Y. Irie, H. Imoto and K. Naka, Synthesis and properties of polyimides containinghexaisobutyl-substituted T8cages in their mainchains, *RSC Adv.*, 2016, **6**, 31751–31757; (*b*) S. Huang and Z. Qiu, Enhanced Thermal Stability and Crystallization Rate of Biodegradable Poly(butylene adipate) by a Small Amount of Octavinyl-Polyhedral Oligomeric Silsesquioxanes, *Ind. Eng. Chem. Res.*, 2014, **53**, 15296–15300; (*c*) H. W. Ro and C. L. Soles, Silsesquioxanes in nanoscale patterning applications, *Mater. Today*, 2011, **14**, 20–33; (*d*) K. Pielichowski, J. Njuguna, B. Janowski and J. Pielichowski, *Polyhedral Oligomeric Silsesquioxanes (POSS)-Containing Nanohybrid Polymers*, Springer, Berlin, Heidelberg, 2006, vol. 201, pp. 225–296.

5 (*a*) Y. R. Liu, Y. D. Huang and L. Liu, Effects of TriSilanolIsobutyl-POSS on thermal stability of methyl-silicone resin, *Polym. Degrad. Stab.*, 2006, **91**, 2731–2738; (*b*) W. Zhang, G. Camino and R. Yang, Polymer/polyhedral oligomeric silsesquioxane (POSS) nanocomposites: An overview of fire retardance, *Prog. Polym. Sci.*, 2017, **67**, 77–125.

6 Y. Kim, K. Koh, M. F. Roll, R. M. Laine and A. J. Matzger, Porous Networks Assembled from Octaphenylsilsesquioxane Building Blocks, *Macromolecules*, 2010, **43**, 6995–7000.

7 H. Ghanbari, B. G. Cousins and A. M. Seifalian, A nanocage for nanomedicine: polyhedral oligomeric silsesquioxane (POSS), *Macromol. Rapid. Commun.*, 2011, **32**, 1032–1046.

8 (*a*) M. Bahrami, J. C. Furgal, H. Hashemi, M. Ehsani, Y. Jahani, T. Goodson, J. Kieffer and R. M. Laine, Synthesis and Characterization of Nanobuilding Blocks $[o\text{-}RStyrPhSiO_{1.5}]_{10,12}$ (R = Me, MeO, NBoc, and CN). Unexpected Photophysical Properties Arising from Apparent Asymmetric Cage Functionalization as Supported by Modeling Studies, *J. Phys. Chem. C*, 2015, **119**(28), 15846–15858; (*b*) T. Zhang, J. Wang, M. Zhou, L. Ma, G. Yin, G. Chen and Q. Li, Influence of polyhedral oligomeric silsesquioxanes (POSS) on blue light-emitting materials for OLED, *Tetrahedron*, 2014, **70**(14), 2478–2486; (*c*) J. C. Furgal, J. H. Jung, S. Clark, T. Goodson and R. M. Laine, Beads on a Chain (BoC) Phenylsilsesquioxane (SQ) Polymers via F– Catalyzed Rearrangements and ADMET or Reverse Heck Cross-coupling Reactions: Through Chain, Extended Conjugation in 3-D with Potential for Dendronization, *Macromolecules*, 2013, **46**(19), 7591–7604; (*d*) K. L. Chan, P. Sonar and A. Sellinger, Cubic silsesquioxanes for use in solution processable organic light emitting diodes (OLED), *J. Mater. Chem.*, 2009, **19**, 9103–9120; (*e*) M. Y. Lo, K. Ueno and H. Tanabe, Silsesquioxane-based nanocomposite dendrimers with photo-luminescent and charge transport properties, *Chem. Rec.*, 2006, **6**, 157–168.

9 (*a*) V. I. Bregadze, Dicarba-*closo*-dodecaboranes $C_2B_{10}H_{12}$ and their derivatives, *Chem. Rev.*, 1992, **92**, 209–223; (*b*) F. Teixidor, C. Viñas, A. Demonceau and R. Núnez, Boron clusters: Do they receive the deserved interest?, *Pure Appl. Chem.*, 2003, **75**, 1305–1313; (*c*) C. Viñas and F. Teixidor, *Science of Synthesis*, Thieme, Stuttgart, 2005, vol. 6, pp. 1235–1275; (*d*) M. Scholz and E. Hey Hawkins, Carbaboranes as Pharmacophores: Properties, Synthesis, and Application Strategies, *Chem. Rev.*, 2011, **111**, 7035–7062; (*e*) F. Issa, M. Kassiou and L. M. Rendina, Boron in Drug Discovery: Carboranes as Unique Pharmacophores in Biologically Active Compounds, *Chem. Rev.*, 2011, **111**, 5701–5722; (*f*) N. S. Hosmane, *Boron Science: New Technologies and Applications*, Taylor & Francis, 2011; (*g*) Z. J. Yao and G. X. Jin, Transition metal complexes based on carboranyl ligands containing N, P, and S donors: Synthesis, reactivity and applications, *Coord. Chem. Rev.*, 2013, **257**, 2522–2535; (*h*) A. M. Spokoyny, New ligand platforms featuring boron-rich clusters as organomimetic substituents, *Pure Appl. Chem.*, 2013, **85**, 903–919; (*i*) J. Zhang and Z. Xie, Synthesis, Structure, and Reactivity of 13- and 14-Vertex Carboranes, *Acc. Chem. Res.*, 2014, **47**, 1623–1633; (*j*) R. N. Grimes, *Carboranes*, Academic Press, US, 3rd edn, 2016; (*k*) N. S. Hosmane and R. Eagling, in *Handbook of Boron Science with Applications in Organometallics, Catalysis, Materials and Medicine*, World Scientific, Singapore, 2019.

10 (*a*) J. Poater, M. Solà, C. Viñas and F. Teixidor, π-Aromaticity and Three-Dimensional Aromaticity: Two sides of the Same Coin?, *Angew. Chem., Int. Ed.*, 2014, **53**, 12191–12195; (*b*) J. Poater, M. Solà, C. Viñas and F. Teixidor, A Simple Link between Hydrocarbon and Borohydride Chemistries, *Chem. – Eur. J.*, 2013, **19**, 4372–4372.

11 (*a*) R. Núñez, P. Farràs, F. Teixidor, C. Viñas, R. Sillanpää and R. Kivekäs, A Discrete P···I-I···P Assembly: The Large Influence of Weak Interactions on the ^{31}P NMR Spectra of Phosphane–Diiodine Complexes, *Angew. Chem., Int. Ed.*, 2006, **45**, 1270–1272; (*b*) A. M. Spokoyny, C. W. Machan, D. J. Clingerman, M. S. Rosen, M. J. Wiester, R. D. Kennedy, C. L. Stern, A. A. Sarjeant and C. A. Mirkin, A coordination chemistry dichotomy for icosahedral carborane-based ligands, *Nat. Chem.*, 2011, **3**, 590–596.

12 (*a*) A. Ferrer-Ugalde, E. J. Juárez-Pérez, F. Teixidor, C. Viñas, R. Sillanpää, E. Pérez-Inestrosa and R. Núñez, Synthesis and Characterization of New Fluorescent Styrene-Containing Carborane Derivatives: The Singular Quenching Role of a Phenyl Substituent, *Chem. – Eur. J.*, 2012, **18**, 544–553; (*b*) A. Ferrer-Ugalde, A. González-Campo, C. Viñas, J. Rodríguez-Romero, R. Santillan, N. Farfán, R. Sillanpää, A. Sousa-Pedrares, R. Núñez and F. Teixidor, Fluorescence of New o-Carborane Compounds with Different Fluorophores: Can it be Tuned?, *Chem. – Eur. J.*, 2014, **20**, 9940–9951; (*c*) C. Bellomo, M. Chaari, J. Cabrera-González, M. Blangetti, C. Lombardi, A. Deagostino, C. Viñas, N. Gaztelumendi, C. Nogués and R. Núñez, Carborane-BODIPY Dyads: New Photoluminescent Materials through

an Efficient Heck Coupling, *Chem. – Eur. J.*, 2018, **24**, 15622–15630; (*d*) A. Ferrer-Ugalde, J. Cabrera-González, E. J. Juárez-Pérez, F. Teixidor, E. Pérez-Inestrosa, J. M. Montenegro, R. Sillanpää, M. Haukka and R. Núñez, Carborane–stilbene dyads: the influence of substituents and cluster isomers on photoluminescence properties, *Dalton Trans.*, 2017, **46**, 2091–2104; (*e*) J. Cabrera-González, S. Bhattacharyya, B. Milián-Medina, F. Teixidor, N. Farfán, R. Arcos-Ramos, V. Vargas-Reyes, J. Gierschner and R. Núñez, Tetrakis{[(p-dodecacarboranyl)methyl]stilbenyl} ethylene: A luminescent tetraphenylethylene (TPE) core system, *Eur. J. Inorg. Chem.*, 2017, 4575–4580.

13 (*a*) A. González-Campo, A. Ferrer-Ugalde, C. Viñas, F. Teixidor, R. Sillanpää, J. Rodríguez-Romero, R. Santillan, N. Farfán and R. Núñez, A versatile methodology for the controlled synthesis of photoluminescent high-boron-content dendrimers, *Chem. – Eur. J.*, 2013, **19**, 6299–6312; (*b*) R. Núñez, M. Tarrés, A. Ferrer-Ugalde, F. F. de Biani and F. Teixidor, Electrochemistry and photoluminescence of icosahedral carboranes, boranes, metallacarboranes, and their Derivatives, *Chem. Rev.*, 2016, **116**, 14307–14378; (*c*) S. Mukherjee and P. Thilagar, Boron clusters in luminescent materials, *Chem. Commun.*, 2016, **52**, 1070–1093.

14 J. Cabrera-González, C. Viñas, M. Haukka, S. Bhattacharyya, J. Gierschner and R. Núñez, Photoluminescence in carborane–stilbene triads: A structural, spectroscopic, and computational study, *Chem. – Eur. J.*, 2016, **22**, 13588–13598.

15 B. P. Dash, R. Satapathy, E. R. Gaillard, K. M. Norton, J. A. Maguire, N. Chug and N. S. Hosmane, Enhanced π-Conjugation and Emission via Icosahedral Carboranes: Synthetic and Spectroscopic Investigation, *Inorg. Chem.*, 2011, **50**, 5485–5493.

16 D. Tu, P. Leong, Z. Li, R. Hu, C. Shi, K. Y. Zhang, H. Yan and Q. Zhao, Carborane-triggered metastable charge transfer state leading to spontaneous recovery of mechanochromic luminescence, *Chem. Commun.*, 2016, **52**, 12494.

17 (*a*) M. Chaari, Z. Kelemen, J. Giner-Planas, F. Teixidor, D. Choquesillo-Lazarte, A. Ben Salah, C. Viñas and R. Núñez, Photoluminescence in *m*-carborane–anthracene triads: a combined experimental and computational study, *J. Mater. Chem. C*, 2018, **6**, 11336–11347; (*b*) M. Chaari, Z. Kelemen, D. Choquesillo-Lazarte, N. Gaztelumendi, F. Teixidor, C. Viñas, C. Nogués and R. Núñez, Efficient blue light emitting materials based on *m*-carborane–anthracene dyads. Structure, photophysics and bioimaging studies, *Biomater. Sci.*, 2019, **7**, 5324–5337.

18 A. Ferrer-Ugalde, E. J. Juárez-Pérez, F. Teixidor, C. Viñas and R. Núñez, Synthesis, characterization, and thermal behavior of carboranyl–styrene decorated octasilsesquioxanes: Influence of the carborane clusters on photoluminescence, *Chem. – Eur. J.*, 2013, **19**, 17021–17030.

19 J. Cabrera-González, A. Ferrer-Ugalde, S. Bhattacharyya, M. Chaari, F. Teixidor, J. Gierschner and R. Núñez, Fluorescent carborane–vinylstilbene functionalised octasilsesquioxanes: synthesis, structural, thermal and photophysical properties, *J. Mater. Chem. C*, 2017, **5**, 10211–10219.

20 (*a*) M. A. Fox, *Icosahedral carborane derivatives*, Durham thesis, Durham University, 1991; (*b*) A. Himmelspach and M. Fince, Dicarba-closo-dodecaboranes with One and Two Ethynyl Groups Bonded to Boron, *Eur. J. Inorg. Chem.*, 2010, 2012–2024.

21 R. H. Grubbs, in *Handbook of Metathesis*, Wiley-VCH, Weinheim, 2003.

22 A. V. Puga, F. Teixidor, R. Sillanpää, R. Kivekääs, M. Arca, G. Barberà and C. Viñas, From Mono- to Poly-Substituted Frameworks: A Way of Tuning the Acidic Character of Cc-H in o-Carborane Derivatives, *Chem. – Eur. J.*, 2009, **15**, 9755–9763.

23 M. Chaari, J. Cabrera-Gonzáñez, Z. Kelemen, C. Viñas, A. Ferrere-Ugalde, D. Choquesillo-Lazarte, A. Ben Salah, F. Teixidor and R. Núñez, Luminescence properties of carborane-containing distyrylaromatic systems, *J. Organomet. Chem.*, 2018, **865**, 206–213.

24 J. R. Lakowicz, *Principles of Fluorescence Spectroscopy*, Springer US, Baltimore, Maryland, USA, 2007.

25 A. M. Brouwer, Standards for photoluminescence quantum yield measurements in solution (IUPAC Technical Report), *Pure Appl. Chem.*, 2011, **83**, 2213–2228.

26 L. Krause, R. Herbst-Irmer, G. M. Sheldrick and D. Stalke, Comparison of silver and molybdenum microfocus X-ray sources for single-crystal structure determination, *J. Appl. Crystallogr.*, 2015, **48**, 3–10.

27 G. M. Sheldrick, A short history of SHELX, *Acta Crystallogr., Sect. A: Found. Crystallogr.*, 2008, **64**, 112–122.

28 O. V. Dolomanov, L. J. Bourhis, R. J. Gildea, J. A. K. Howard and H. Puschmann, OLEX2: a complete structure solution, refinement and analysis program, *J. Appl. Crystallogr.*, 2009, **42**, 339–341.

